Songklanakarin J. Sci. Technol.
36 (2), 217-225, Mar. - Apr. 2014

SJST SONGKLANAKARIN JOURNAL OF SCIENCE AND TECHNOLOGY
http://www.sjst.psu.ac.th

Original Article

Core-SOL simulations of *L*-mode tokamak plasma discharges using BALDUR code

Yutthapong Pianroj [1]* and Thawattchai Onjun [2]

[1] *Program in Industrial Management Technology, Faculty of Sciences and Industrial Technology, Prince of Songkla University, Surat Thani Campus, Mueang, Surat Thani, 84000 Thailand.*

[2] *School of Manufacturing Systems and Mechanical Engineering, Sirindhorn International Institute of Technology, Thammasat University, Khlong Luang, Pathum Thani, 12121 Thailand.*

Received 20 May 2013; Accepted 12 November 2013

Abstract

Core-SOL simulations were carried out of plasma in tokamak reactors operating in a low confinement mode (*L*-mode), for various conditions that match available experimental data. The simulation results were quantitatively compared against experimental data, showing that the average RMS errors for electron temperature, ion temperature, and electron density were lower than 16% or less for 14 *L*-mode discharges from two tokamaks named DIII-D and TFTR. In the simulations, the core plasma transport was described using a combination of neoclassical transport calculated by NCLASS module and anomalous transport by Multi-Mode-Model version 2001 (MMM2001). The scrape-off-layer (SOL) is the small amount of residual plasma that interacts with the tokamak vessel, and was simulated by integrating the fluid equations, including sources, along open field lines. The SOL solution provided the boundary conditions of core plasma region on low confinement mode (*L*-mode). The experimental data were for 14 *L*-mode discharges and from two tokamaks, named DIII-D and TFTR.

Keywords: tokamak, fusion, *L*-mode, SOL, and tokamak plasma

1. Introduction

The low confinement mode (*L*-mode) is an operating regime of particular interest for burning plasma experiments in the magnetic confinement fusion concept. While the performance in *L*-mode is lower than in high confinement mode (*H*-mode), when the plasmas are heated with the same input power, the *H*-mode operation is often perturbed by discharges that are quasi-periodic bursts of energy and particles near the edge of the plasma. This activity is referred to as "*edge localized modes*" (ELMs), and each ELM burst results in a rapid loss of particles and energy at the plasma boundary, which can damage tokamak wall or components. The confined plasma should pass the *L*-mode before reaches the *H*-mode and *L*-mode is more stable and easier to control than the *H*-mode, thus an improved understanding of *L*-mode operation could potentially improve its performance, and such understanding is sought in the form of validated numerical simulation models.

The goal of the current study is to demonstrate improvements in the numerical simulation of *L*-mode operation, the plasma parameters, such as, temperature, density, particle and thermal diffusivities, and the accuracy in matching available experimental data. Normally, the tokamak plasma can be divided into three main regions, as shown in Figure 1. The core plasma region is the main part of the plasma, extending from its center to the edge region close to separatrix. The plasma confined in the core region produces the fusion energy. The edge plasma region is narrow, and is located between the core region and the separatrix. In

* Corresponding author.
Email address: yutthapong.p@psu.ac.th

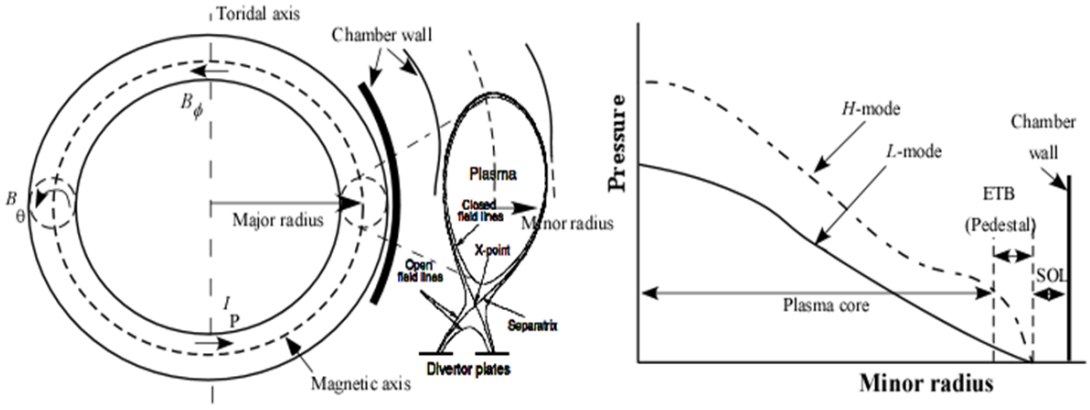

Figure 1. Geometric sketch of tokamak illustrates the technical terms used in the text. The major radius is measured from the toroidal axis to the geometric center of the plasma, while the minor radius is measured from the geometric center to the edge of the plasma. The magnetic field consist of two components: a toroidal magnetic field B_ϕ, and a poloidal magnetic field B_θ. The graph on right shows the pressure profiles along normalized minor radius, for *L*-mode and *H*-mode operation. The three main regions of tokamak plasma, plasma core, edge (pedestal), and SOL, are indicated.

H-mode operation, normally, a transport barrier is formed in the edge region. The edge transport barrier (ETB) is characterized by sharp temperature and density gradients, and is also called the "pedestal". However, when a tokamak is operated in *L*-mode, no pedestal is formed because the total power is lower than the threshold power (Connor *et al.*, 2000). The scrape-off-layer (SOL) is the region outside of the last closed magnetic flux surface or separatrix, and the magnetic field lines in it run into the limiter or diverter. The SOL plasma is essentially governed by two-dimensional effects, such as the flows of heat and particles along and across the magnetic field lines. The physics of the SOL are affected by atomic processes and plasma-wall interactions. In the boundary layer of SOL the plasma flows along the magnetic field and then interacts with a solid surface. Ions may then be neutralized and backscattered or released to re-enter the plasma. This process is known as "*recycling*".

The importance of SOL is that it acts as both sink and source of energy and particles in tokamak plasma, determining the boundary conditions for the plasma core area. The BALDUR integrated predictive modeling code includes both particle and heat-loss models at the SOL, known as a 'two chambers model' (Langer *et al.*, 1985), the source terms due to neutral gas, and neutral beam injection are computed; moreover, the neoclassical and anomalous parts of particle and heat transport in the plasma core are simulated by the NCLASS module (Houlberg *et al.*, 1997) and the Multi-mode version 2001 (MMM2001), respectively.

With these combined elements, we carried out simulations of prior experiments that concentrate on systematic scans of *L*-mode discharges in the Doublet III Device (DIII-D) (Luxon *et al.*, 1985) tokamak and the Tokamak Fusion Test Reactor (TFTR) (Grove *et al.*, 1985); particularly experiments with scans of gyro-radius (Kinsey *et al.*, 1996), plasma power, current, and density (Kinsey *et al.*, 1996). Reporting this work is organized as follows: a brief description of the BALDUR code is given in the next section, and then the SOL model, the neoclassical transport NCLASS module and the anomalous core transport MMM2001 are also briefly described. In Section 4, the simulations for standard *L*-mode are validated by quantitative comparisons to the experimental data, before the final conclusions.

2. Code and Model Descriptions

2.1 BALDUR Integrated predictive modeling code

The self-consistency integrated predictive modeling code named BALDUR (Redi *et al.*, 1991; Singer *et al.*, 1988) is based on a 1.5 dimensional code where the transport equations are one-dimensional flux-surface-averaged equations, in which metric elements describe the effects of the two dimensional shapes on the magnetic flux surfaces. The 1.5 dimensional code assumes that the magnetic flux surfaces are closed and the transport along magnetic field lines is much larger than the transport across the field lines. BALDUR uses theory-based and empirical models to compute self-consistently the source neutral beam injection (NBI) heating, nuclear reaction, radio frequency (RF heating), sink (impurity radiation), energy and particle transport fluxes, magnetohydrodynamic equilibrium, and large scale instabilities (sawtooth oscillations). The BALDUR simulations have been used to predict the time evolution of plasma profiles including electron and ion temperature, hydrogen and impurity densities, safety factor, neutrals and fast ions, for *L*-mode and *H*-mode discharges of conventional tokamaks. BALDUR simulations have been extensively compared with experimental data on plasma, and have yielded overall agreements with about a 10% relative RMS deviation (Hannum *et al.*, 2001; Onjun *et al.*, 2001).

A brief description of BALDUR code is described above. It was developed by FORTRAN language, which

contains many sub-modules or subroutines inside. The initial input file is generated based on details from the experiment, such as engineering parameters, diagnostic time, and types of heating power. Then the SOL module calculates and provides the initial and boundary conditions to the core area. In this area, the thermal and particle transports are calculated by using NCLASS module and MMM2001 to calculate neoclassical and anomalous transports, respectively. In the next subsection, the brief description of SOL, NCLASS, and MMM2001 modules will be described, respectively.

2.2 Particle and heat-loss model at SOL

Plasma transport models of radial flow in tokamaks with a diverter or pumped limiter must include particle and heat-loss terms due to flow along magnetic-field lines in the SOL. The plasma entering the SOL flows along open field lines until it reaches the neutralizer plate. The resulting neutral gas interacts with the incoming plasma and modifies its properties and flow. The greatest effect occurs when there is a large recycling of the neutral gas. This happens when the neutrals are ionized by the plasma near the neutralizer and are swept back to the neutralizer, and this cycle is repeated. This enhancement of the plasma flow near the neutralizing surface serves to amplify the particle flux and reduce the temperature, thereby minimizing erosion. The amplification of particle flux due to recycling also reduces the upstream plasma flow velocity along the field lines in the SOL, thus changing the edge density of the main plasma region. To solve the flow of material entering from the SOL into the high-recycling region, all radial flows are ignored and consider only parallel flow along the field lines. This is because the BALDUR considers the radial flow in SOL.

In summary, the SOL model takes account of loss due to the parallel flow to the divertor, and the loss terms are derived from 1D fluid equations (including source terms) along the magnetic field line for simplicity; therefore, the radial-transport modeling from the magnetic axis to the wall is described by BALDUR code and loss terms due to the SOL parallel flow are included from the separatrix to the wall that is shown in previous works (Singer, 1984; Singer *et al.*, 1982).

2.3 Neoclassical transport model

The NCLASS module (Houlberg *et al.*, 1997) calculates the neoclassical transport properties of multi-species axisymmetric plasma of arbitrary aspect ratio, geometry and collisionality. The neoclassical effects refer to the flows resulting from Coulomb collisions between particles drifting in non-uniform magnetic and electric fields. This module determines a multi-fluid model for the parallel and radial force balance equations, giving the neoclassical bootstrap current, parallel electrical resistivity, impurity and fuel ion radial particle transport, ion radial thermal transport and plasma poloidal rotation. It is designed to be called from a transport code that provides the plasma density, temperature profiles, and a number of flux surface averaged geometric quantities.

2.4 Anomalous core transport model

The Multi-Mode Model version 2001 (MMM2001) is a combination of theory-motivated transport models used to predict plasma profiles in tokamaks. It consists of the Weiland model for the ion temperature gradient (ITG) and trapped electron modes (TEM) (Nilsson *et al.*, 1994; Nordman *et al.*, 1990; Weiland *et al.*, 1992), the Guzdar-Drake model for drift-resistive ballooning modes (Guzdar *et al.*, 1993; Kinsey *et al.*, 1996), and kinetic ballooning modes (Bateman *et al.*, 1998). Usually, the Weiland model for drift modes provides the largest contribution, followed by drift-resistive ballooning (RB) and kinetic ballooning (KB) modes. The Weiland model is derived by linearizing the fluid equations, with magnetic drifts for each plasma species. Eigenvalues and eigenvectors computed from these fluid equations are then used to compute a quasi-linear approximation for the thermal and helium transport fluxes. The Weiland model includes many different physical phenomena such as effects of trapped electrons, unequal ion and electron temperatures, impurities, fast ions, finite plasma pressure (β), and collisions. The resistive ballooning model in the MMM2001 transport model is based on the $E\times B$ drift-resistive ballooning mode model by Guzdar-Drake *et al.* (1993), in which the transport is proportional to the pressure gradient and collisionality. The contribution from the resistive ballooning model usually dominates the transport near the plasma edge. The kinetic ballooning model is semi-empirical, and usually provides a small contribution to the total diffusivity throughout the plasma, except near the magnetic axis. However, the kinetic ballooning model plays quite a significant role in the region near the plasma core up to some radius. This model is an approximation to the first ballooning mode stability limit. All the anomalous transport contributions to the MMM2001 transport model are multiplied by the inverse fourth power of the plasma elongation (κ^{-4}) (Bateman *et al.*, 1998), since the models were originally derived for circular plasmas. The expressions of the calibration coefficients and transport coefficients in MMM2001 (Kinsey *et al.*, 1996) are:

$$\chi_i = 0.8\chi_{i_{ITG\&TEM}} + 1.0\chi_{i_{RB}} + 1.0\chi_{i_{KB}} \quad (1)$$

$$\chi_e = 0.8\chi_{e_{ITG\&TEM}} + 1.0\chi_{e_{RB}} + 1.0\chi_{e_{KB}} \quad (2)$$

$$D_H = 0.8D_{H_{ITG\&TEM}} + 1.0D_{H_{RB}} + 1.0D_{H_{KB}} \quad (3)$$

$$D_Z = 0.8D_{Z_{ITG\&TEM}} + 1.0D_{Z_{RB}} + 1.0D_{Z_{KB}} \quad (4)$$

where, χ_e is the electron diffusivity, χ_i is the ion diffusivity, D_H is the hydrogenic particle diffusivity, D_Z is the impurity diffusivity, $\chi_{ITG\&TEM}$ is the thermal diffusivity of ion temperature gradient and trapped electron mode, χ_{RB} is the resistive ballooning thermal diffusivity, and χ_{KB} is the kinetic ballooning thermal diffusivity.

Table 1. List of discharges with ρ^* scans.

Tokamak	DIII-D			TFTR		
Discharge ID	78281	78106	78283	50921	50904	50911
Type of heating	RF	RF	NBI	NBI	NBI	NBI
Major radius, R (m)	1.70	1.70	1.69	2.45	2.45	2.45
Minor radius, a (m)	0.628	0.629	0.618	0.797	0.798	0.798
Plasma elongation, κ	1.84	1.87	1.86	1.00	1.00	1.00
Plasma delta, δ	0.60	0.60	0.60	0.00	0.00	0.00
Toroidal magnetic field, (T)	1.00	2.00	1.00	2.14	2.86	4.23
Plasma current, I_p (MA)	0.58	1.00	0.465	0.890	1.19	1.78
Line average density, $\overline{n}_e(10^{19}\,\mathrm{m}^{-3})$	1.39	3.78	1.20	1.77	2.73	4.37
Effective charge, Z_{eff}	2.5	2.1	2.45	2.24	2.05	1.79
Auxiliary heating power, (MW)	0.38	1.5	0.51	4.66	7.31	17.72
Diagnostic time (sec)	2.60	2.55	3.90	3.95	3.95	3.93

Table 2. List of discharges with engineering parameter scans, using NBI heating for the TFTR tokamak.

Discharge ID	45966	45984	46290	52182	62270	88574	88742	105290
R (m)	2.45	2.45	2.45	2.45	2.45	2.45	2.45	2.45
a (m)	0.80	0.87	0.90	0.87	0.80	0.95	0.88	0.95
κ	1.00	1.00	1.00	1.00	1.00	1.00	1.00	1.00
δ	0.00	0.00	0.00	0.00	0.00	0.00	0.00	0.00
B_T(T)	4.76	4.76	4.76	4.74	4.77	4.75	4.75	4.75
I_P(MA)	2.00	2.00	2.00	0.94	1.78	2.27	2.27	1.98
$\overline{n}_e(10^{19}\,\mathrm{m}^{-3})$	3.44	3.51	4.01	4.75	3.23	4.75	4.72	4.87
Z_{eff}	2.30	2.20	3.40	1.67	2.91	1.78	1.85	1.24
P_{NB} (MW)	11.3	10.82	10.80	10.5	19.2	16.40	17.17	13.86
Diagnostic time (sec)	3.47	5.00	5.00	5.00	4.17	4.62	3.85	4.5

3. Simulation Results and Discussion

3.1 Profile comparison

The predicted plasma profiles were obtained from BALDUR for 14 *L*-mode discharges obtained from either DIII-D or TFTR tokamaks. The ion and electron temperature and the electron density profiles from these simulations were compared with experimental data. Table 1 and 2 show all the discharges that were simulated, together with their global plasma parameters. The first table lists those discharges that included normalized gyro-radius (ρ^*) scans, while the second lists those discharges that included engineering scans (i.e., scans in plasma current, density, heating power, isotope, and others). The tables list the tokamak name, discharge ID number, type of systematic scan, type of auxiliary heating plasma parameters, and diagnostic time. The boundary conditions for temperature and density at the wall were set at 1 eV (1eV = 11,604 K) and $1\times10^{17}\,\mathrm{m}^{-3}$, respectively. However, the effects of temperature and density at the boundary were investigated in Figure 2. In this figure, the temperatures at the boundary were set to 1, 10, 50, and 100 eV, also the densities at the boundary were set to 110^{17}, 1010^{17} 5010^{17}, and $10010^{17}\mathrm{m}^{-3}$ to study the sensitivity of Core-SOL simulations. These effects had small effects to the whole plasma profiles.

Figure 3 shows the simulated profiles obtained Core-SOL BALDUR simulations compared against experimental data in high ρ^* scan (left panel) and low ρ^* scan (right panel). As described in Kinsey *et al.* (1996), the heating power, plasma density, magnetic field, and plasma current were changed from one discharge to the next in these scans, so that the central values of plasma pressure (β) and collisionality were held constant while the number of gyro-radii across the plasma varied. For the high ρ^* scan discharge case (discharge 50921), the simulated electron temperature, ion temperature, and electron density fit the experimental data well from the outer core to the edge area (normalized minor radius (r/a) = 0.3-1.0). However, at the core center (r/a = 0.0–0.3), the simulation of ion temperature is not a good match

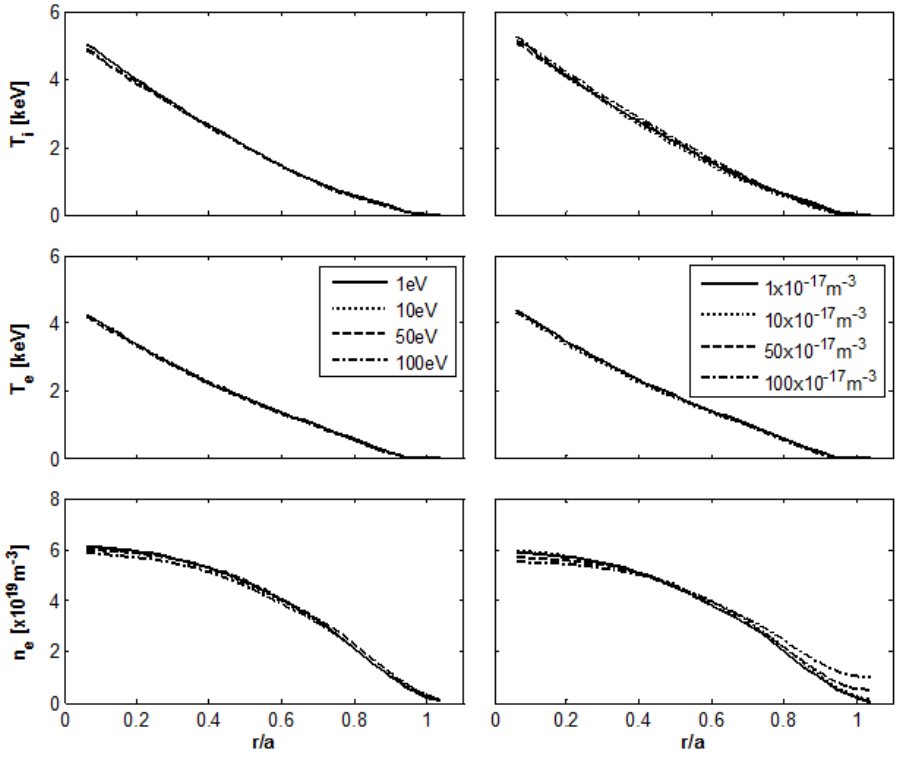

Figure 2. Plots for assessing the sensitivity to SOL boundary conditions, in simulations of TFTR tokamak device, discharge 50911. On the left side, the ion temperature, electron temperature, and electron density are plotted as functions of normalized minor radius, with various temperatures at the boundary. On the right side, the ion temperature, electron temperature, and electron density are plotted as functions of normalized minor radius, with various densities at the boundary.

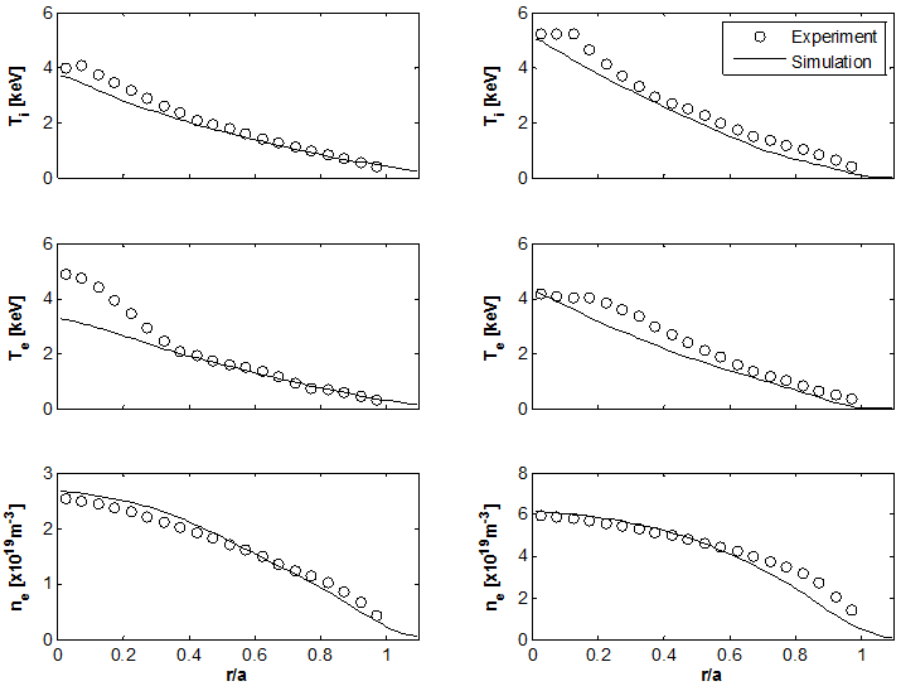

Figure 3. Ion temperature, electron temperature, and electron density as functions of normalized minor radius, from simulation of the high ρ^* discharge TFTR 50921(left side) and from simulation of the low ρ^* discharge TFTR 50911 (right side). The circles represent experimental data while the solid curves are simulation results, using the MMM2001 and the SOL modules.

to the experiment. On the right side plots of the figure, the simulations fit the experiment quite well, for the low ρ^* scan discharge case with numeric ID 50911.

The profiles in Figure 4 are for discharges in a ρ^* scan in DIII-D with RF heating. On the left panels, they stand for high ρ^* discharge 78281 and low ρ^* discharge 78106 on the right panels. The simulations with MMM2001 core transport model and SOL module, using BALDUR code, matched experimental data poorly. Especially the core region for both DIII-D discharges shows lack of fit. These subjective facts were confirmed by statistical analysis as discussed in the next section. In Figure 5, the profile results are the ion, electron thermal diffusivities, and hydrogenic particle diffusivity from the BALDUR simulation plotted as a function of normalized minor radius. Note that these diffusivities are obtained from the simulations and not from the experimental data. On the left panels, they show the diffusivities for the low ρ^* TFTR discharge 50911 and the high ρ^* DIII-D discharge 78106 is shown on the right panels. Indicated are the contributions from each of the modes to the thermal and particle transport. The total diffusivity is shown with a thick solid line. In the core area, the transport is dominated by the ion temperature gradient (itg) mode but the resistive ballooning (rb) mode dominates at the edge to the SOL region for both thermal diffusivities and particle diffusivity. In the case of kinetic ballooning (kb) mode, it is the least significant in thermal and particle transport coefficients when compares to other modes.

3.2 Statistical analysis

To quantify the comparison between simulations and experiments, for 14 *L*-mode TFTR and DIII-D discharges, the percentage of root-mean-square (RMS [%]) deviations were computed between the simulated profiles and experimental data. The RMS [%] defined by Equation (5) has been used in previous studies (Hannum *et al.*, 2001; Onjun *et al.*, 2002; Pianroj *et al.*, 2012; Pianroj *et al.*, 2012) and was also used here.

$$\mathrm{RMS}[\%] = \sqrt{\frac{1}{N}\sum_{i=1}^{N}\left(\frac{x_{sim_i} - x_{\exp_i}}{x_{\exp_0}}\right)^2} \times 100 \qquad (5)$$

where, $x_{\exp_i}$ is the i^{th} data point of the experimental profile, x_{sim_i} is the corresponding value from the simulated profile, $x_{\exp_0}$ is the maximum value in the experimental profile, and there are *N* points in total. The offset [%] is defined by

$$\mathrm{offset}[\%] = \frac{1}{N}\sum_{i=1}^{N}\left(\frac{x_{sim_i} - x_{\exp_i}}{x_{\exp_0}}\right) \times 100 \qquad (6)$$

A positive (negative) offset indicates that the simulated profile is predominantly higher (lower) than the experimental profile. Figures 6 and 7 show the RMS [%] and offset [%] for the 14 *L*-mode discharges. The RMS of electron temperature ranges from 4.28% to 21.89% with an 11.79% average. The offset of electron temperature is mostly

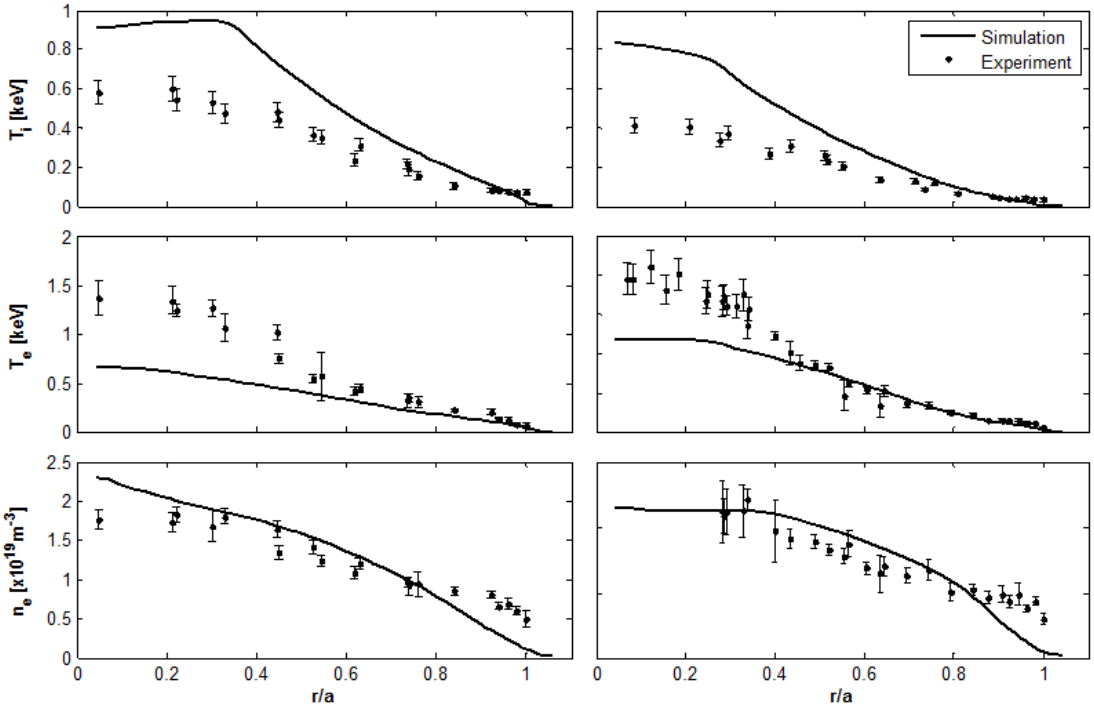

Figure 4. Ion temperature, electron temperature, and electron density as functions of normalized minor radius for the high ρ^* discharge with ID 78281(left side) and for the low ρ^* discharge with ID 78106 (right side), in DIII-D tokamak. The filled circles represent experimental data while the solid curves are from a simulation using the MMM2001 model and the SOL module.

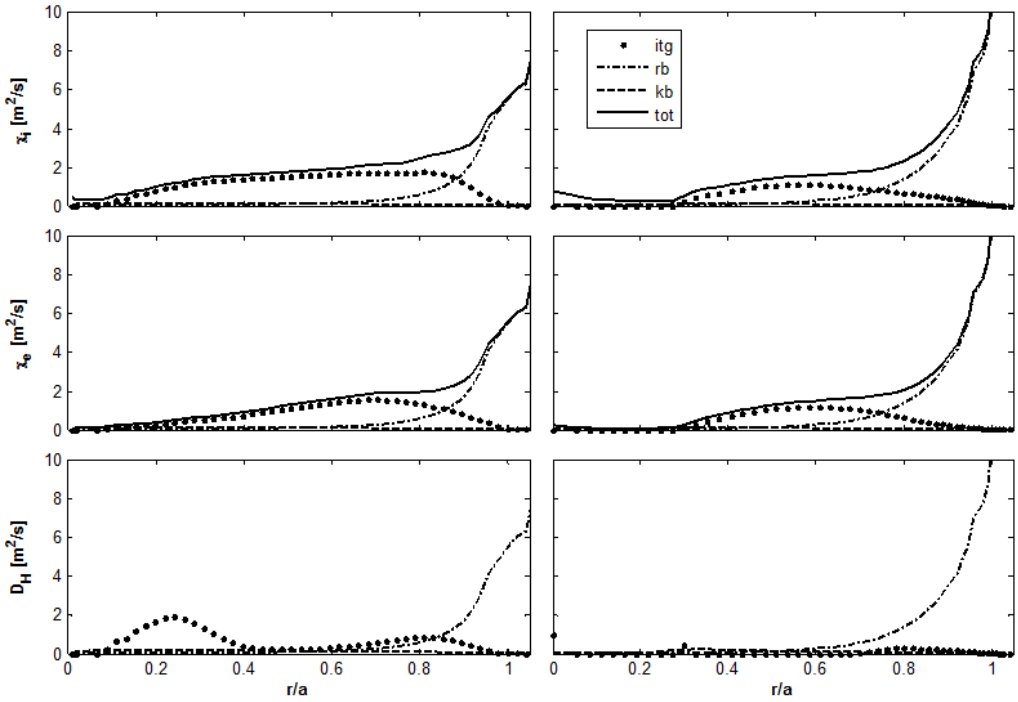

Figure 5. Contributions to effective diffusivities from the MMM2001 core transport model, in simulations of the low ρ^* discharge TFTR 50911 (on left) and the low ρ^* discharge DIII-D 78106 (on right). For the ion thermal diffusivity in the top row and the electron thermal diffusivity in the middle row, the dotted line shows the (itg) contribution, the dashed-dotted line shows the resistive ballooning (rb) contribution, the dashed line shows the kinetic ballooning (kb) contribution, and the solid line shows the total effective diffusivity (tot). The anomalous part of the hydrogenic ion diffusivity is shown in the bottom row of plots.

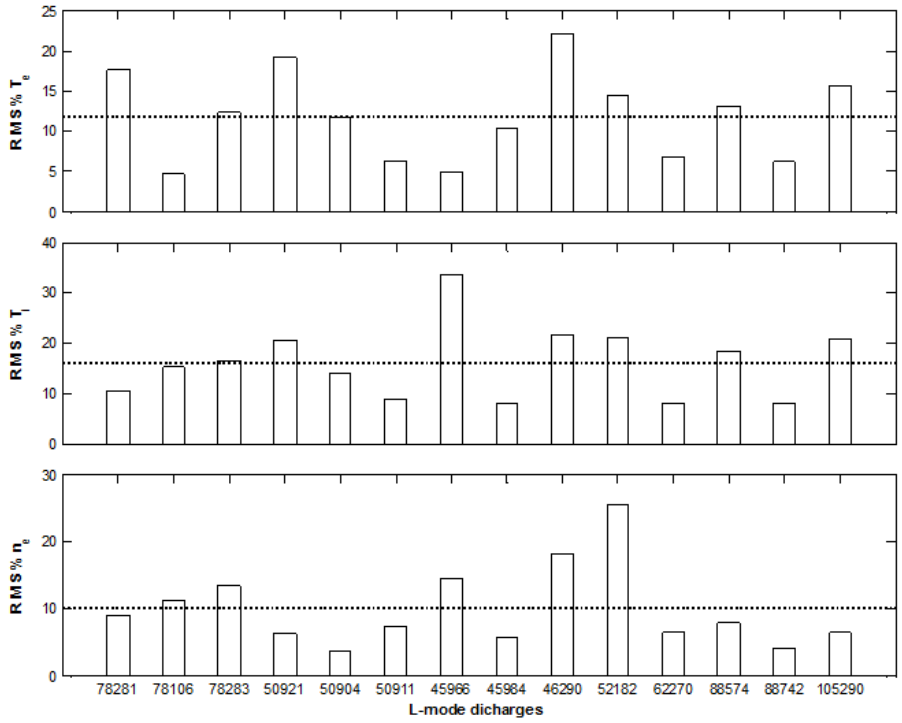

Figure 6. Root mean square deviations (%RMS) from experiments, for the simulated electron temperature, ion temperature, and electron density profiles. These simulations, of 14 *L*-mode discharges in the DIII-D and TFTR tokamak devices. The dashed lines show the RMS% averages across all the discharges, in each plot.

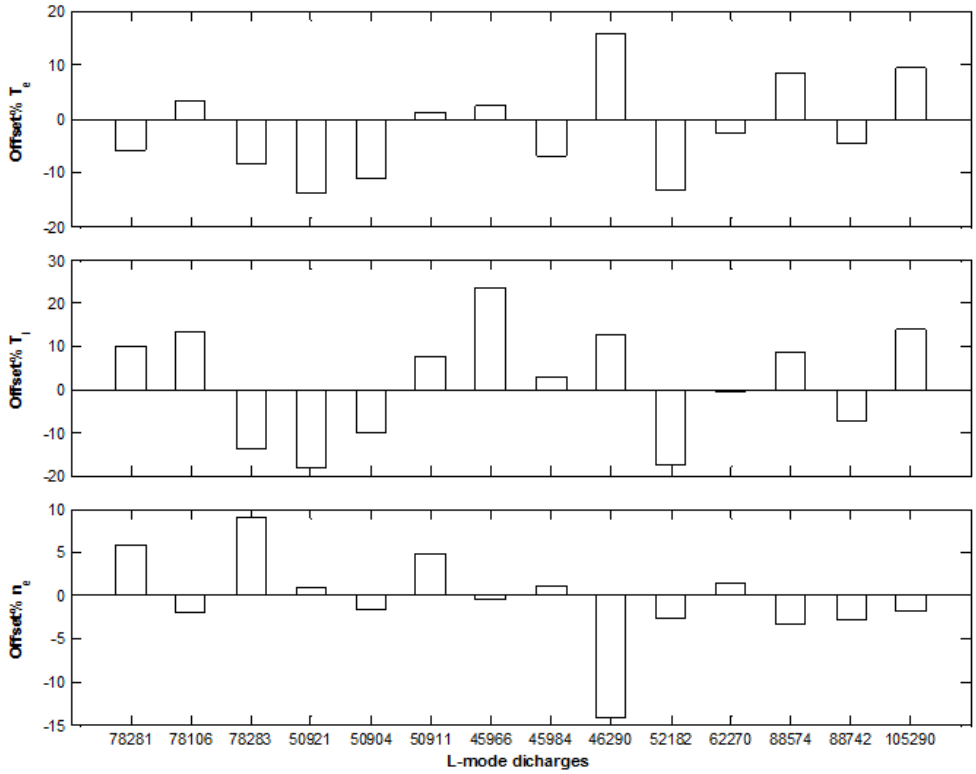

Figure 7. Plots of the offsets (%offset, see text for definition) of the electron temperature, ion temperature, and electron densities, for the 14 *L*-mode discharges.

negative, indicating that simulations tend to under-predict the experimental data. For the ion temperature the RMS ranges from 7.27% to 32.52% with 16.08% average, with mostly positive offsets. This indicates that the simulations tend to over-predict the ion temperatures. Finally, for the electron density the RMS ranges from 2.87% to 23.56% with 9.97% average and mostly negative offsets, indicating that simulations under-predict the experiments.

4. Conclusions

Simulations of tokamak plasma were carried out with BALDUR code, with the multi-mode anomalous core transport model version 2001 (MMM2001) coupled with a sink and source model for particles in the SOL region. Experimental results for a total of 14 discharges in the TFTR and DIII-D tokamaks, operated in *L*-mode regime, were compared to simulations. Quantitative assessment of the deviations between simulations and experiments was based on the RMS of deviations. The average RMS deviations were about 12% for electron temperature, 16% for ion temperature, and 10% for electron density.

Acknowledgements

The author gratefully thanks Assoc. Prof. Sappo Karrila, for his assistance in manuscript preparation. This work is supported by Prince of Songkla University research fund under contract number PSU 166/3249, which is gratefully acknowledged.

References

Bateman, G., Kritz, A.H., Kinsey, J.E., Redd, A.J. and Weiland, J. 1998. Predicting temperature and density profiles in tokamaks. Physics of Plasmas. 5, 1793-1799.

Connor, J.W. and Wilson, H.R. 2000. A review of theories of the L-H transition. Plasma Physics and Controlled Fusion. 42, R1-R74.

Grove, D.J. and Meade, D.M. 1985. Initial studies of confinement, adiabatic compression, and neutral-beam heating in TFTR. Nuclear Fusion. 25, 1167.

Guzdar, P.N., Drake, J.F., McCarthy, D., Hassam, A.B. and Liu, C.S. 1993. Three-dimensional fluid simulations of the nonlinear drift-resistive ballooning modes in tokamak edge plasmas. Physics of Fluids B: Plasma Physics. 5, 3712-3727.

Hannum, D., Bateman, G., Kinsey, J., Kritz, A.H., Onjun, T. and Pankin, A. 2001. Comparison of high-mode predictive simulations using Mixed Bohm/gyro-Bohm and Multi-Mode (MMM95) transport models. Physics of Plasmas. 8, 964-974.

Houlberg, W.A., Shaing, K.C., Hirshman, S.P. and Zarnstorff, M.C. 1997. Bootstrap current and neoclassical trans-

port in tokamaks of arbitrary collisionality and aspect ratio. Physics of Plasmas. 4, 3230.

Kinsey, J.E. and Bateman, G. 1996. Theory-based transport modeling of the gyro-radius experiments. Physics of Plasmas. 3, 3344-3357.

Kinsey, J.E., Bateman, G., Kritz, A.H. and Redd, A. 1996. Comparison of two resistive ballooning mode models in transport simulations. Physics of Plasmas. 3, 561-570.

Langer, W.D. and Singer, C.E. 1985. Two-Chamber Model for Diverters with Plasma Recycling. Institute of Electrical and Electronics Engineers (IEEE) Transactions on Plasma Science. PS-13, 163-166.

Luxon, J.L. and Davis, L.G. 1985. Big Dee: A flexible facility operating near breakeven conditions. Fusion Technology. 8, 441.

Nilsson, J. and Weiland, J. 1994. Fluid model for general collisionality and magnetic curvature. Nuclear Fusion. 34, 803.

Nordman, H., Weiland, J. and Jarmén, A. 1990. Simulation of toroidal drift mode turbulence driven by temperature gradients and electron trapping. Nuclear Fusion. 30, 983.

Onjun, T., Bateman, G. and Kritz, A.H. 2001. Comparision of low confinement mode transport simulation using mixed Bohm/gyro-Bohm and the Multi-Mode 95 transport model. Physics of Plasmas. 8, 975.

Onjun, T., Bateman, G. and Kritz, A.H. 2002. Models for the pedestal temperature at the edge of H-mode tokamak plasmas. Physics of Plasmas. 9, 5018-5030.

Pianroj, Y. and Onjun, T. 2012. Simulations of H-mode Plasma in Tokamak Using a Complete Core-Edge Modeling in the BALDUR Code. Plasma Science and Technology. 14, 778-788.

Pianroj, Y., Techakunchaiyanunt, J. and Onjun, T. 2012. Model for Pedestal Transport Based on Suppression of Anomalous Transport Using ω_{ExB} Flow Shear and Magnetic Shear. Journal of the Physical Society of Japan. 81, 1-13.

Redi, M.H. and Bateman, G. 1991. Transport simulations of TFTR experiments to test theoretical models for χ e and χ i. Nuclear Fusion. 31, 547.

Singer, C.E. 1984. The H-mode transition. Plasma Physics Laboratory, Applied Physics Division, Princeton University. Report. 27.

Singer, C.E. and Langer, W.D. 1982. Axisymmetric tokamak scapeoff transport, PPPL-1920, 1- 42.

Singer, C.E., Post, D.E., Mikkelsen, D.R., Redi, M.H., McKenney, A., Silverman, A., Seidl, F.G.P., Rutherford, P.H., Hawryluk, R.J., Langer, W.D., Foote, L., Heifetz, D.B., Houlberg, W.A., Hughes, M.H., Jensen, R.V., Lister, G. and Ogden, J. 1988. Baldur: A one-dimensional plasma transport code. Computer Physics Communications. 49, 275-398.

Weiland, J. and Hirose, A. 1992. Electromagnetic and kinetic effects on the ion temperature gradient mode. Nuclear Fusion. 32, 151.